INFLUENCE OF DOPING PROFILE OF HIGHLY DOPED REGIONS FOR SELECTIVE EMITTER SOLAR CELLS

Ulrich Jäger, Sebastian Mack, Achim Kimmerle, Andreas Wolf and Ralf Preu
Fraunhofer Institute for Solar Energy Systems (ISE), Heidenhofstrasse 2, D-79110 Freiburg, Germany

ABSTRACT

The influence of the doping profile under the metallization for laser doped selective emitter solar cells is investigated. Laser doping allows profile tailoring to some extent by adapting the pulse energy, resulting in Gaussian doping profiles. Numerical calculations using PC1D show that the doping profile influences the recombination at the metal-semiconductor interface. The value $J_{0e,met}$ is used to characterize this influence on solar cell level employing calculations with the 2-diode-model. Selective emitter solar cells have been fabricated to validate, whether this effect can be observed on cell level. IV measurements show a dependence of the open circuit voltage on the profile. This is determined to be partly due to a different 2nd diode recombination current J_{02} for different doping profiles underneath the contact. The effect of $J_{0e,met}$ is also ascertainable.

INTRODUCTION

Selective emitters offer the opportunity to boost cell efficiency in a comparable simple way. A low doping is chosen in the photoactive area, to reduce recombination losses and increase blue response. Underneath the contacts, a highly doped emitter is chosen to ensure a good metal semiconductor contact and provide some shielding of the minorities from the contact.
Laser doping from phosphosilicate glass (PSG) [1-3] offers the possibility to implement a selective emitter in a fast and cost effective way, by introducing a single laser processing step after furnace diffusion. This doping process is characterized by a classical diffusion from a limited doping source, thus resulting in a Gaussian doping profile after resolidification.

LASER DOPED PROFILES

Laser Doping

Laser doping can be regarded as finite source diffusion, yielding Gaussian doping profiles after resolidification. The impurity concentration C after a time t in the depth z is given by

$$C(z,t) = \frac{Q}{\sqrt{\pi D t}} \exp\left(\frac{-z^2}{4Dt}\right) \qquad (1)$$

With Q as the total amount of impurities and the diffusion constant D. Larger pulse energies lead to deeper and longer melting [4], thus lowering the impurity surface concentration, as eq. (1) implicates. This is shown in Figure 1 exemplarily. Four different melting times and thus doping depths are depicted for a constant value of $Q = 6\text{x}10^{15}$ cm^{-2} of phosphorus. The corresponding sheet resistances for a p-type 1 Ωcm wafer are calculated through

$$R_{sheet} = \int_0^W \frac{dz}{e \cdot \mu_n(N,z) \cdot N(z)} \qquad (2)$$

using the mobilities μ_n of the program PC1D [5]. Further, the elementary charge is denoted by e, W is the junction depth and N the impurity density in the emitter region. It is assumed that all dopant atoms are electrically active. At high doping concentrations above $N = 4\text{x}10^{20}$ cm^{-3} this assumption may not valid due to possible clustering of phosphorus atoms. This may be the case in the shallow doping profile, however authors have reported electrically active dopants above the solid solubility limit [6] after laser annealing to the high temperatures and fast recrystallization [7].

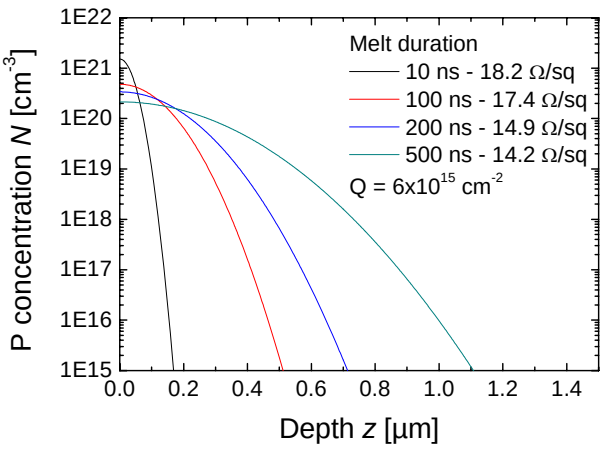

Figure 1: Gaussian doping profiles for different melting times and a constant amount of impurities Q according to eq. (1). The corresponding sheet resistances for each curve are also given.

Shielding of the minorities from the contact

To quantify the impact of a pulse variation in the laser doping process for selective emitter formation on the shielding of the minorities from the contact, numerical simulation has been conducted with the program PC1D Version 5.9. The aim was to extract a value, characterizing the recombination underneath the metal contact. Thus, the emitter saturation current density of a metalized surface, labeled as $J_{0e,met}$ in the following, was calculated for a device in open circuit condition with a homogeneous generation of carriers of 35 mA/cm². A recombination velocity of the carriers at the metalized front side $S_{p0} = 10^7$ cm/s was assumed, with no recombination taking place at the rear or in the bulk. A random pyramid texture and a Gaussian phosphorus emitter doping profile were placed at the front side of the p-type, 2 Ωcm, 250 µm thick device. Thus all recombination takes place in the emitter and at the front side. A variation in the depth and the surface concentration N_{surf} of the emitter was investigated and the open circuit voltage of the device was extracted. The emitter saturation current density $J_{0e,met}$ was calculated through the 1-diode model

$$J_{0e,met} = J_{SC} \cdot \left(\exp\left(\frac{eV_{OC}}{kT} \right) - 1 \right)^{-1} \qquad (3)$$

With J_{SC} = 35 mA/cm² being the total current generated in the device and contributing to the recombination at a temperature of T = 300 K. The result is shown in Figure 2.

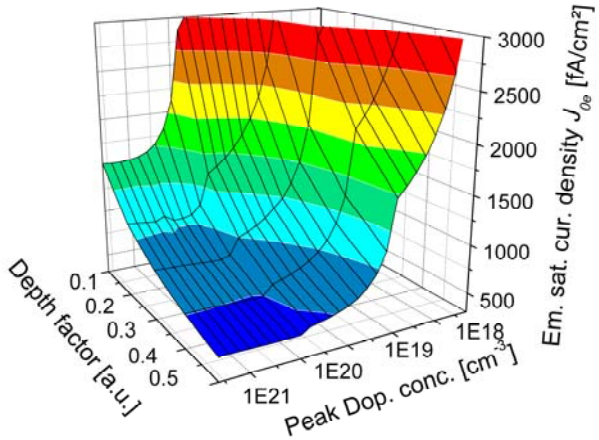

Figure 2: Calculated emitter saturation current densities of metalized surfaces $J_{0e,met}$ as a function of peak doping concentration N_S and the depth factor of the Gaussian profile

A clear trend can be seen. A high peak doping concentration and deep junction is strongly beneficial for the reduction of $J_{0e,met}$. This trend has also been reported by other authors [8, 9]. The minimum values for $J_{0e,met}$ that are obtained for the depth factors of the Gaussian profiles are summarized in Table I.

	Min. $J_{0e,met}$ [fA/cm²]	At Peak Doping N_{surf} [cm^{-3}]	Junction depth [µm]	R_{sheet} [Ω/sq]
0.1	1520	$8x10^{20}$	0.330	13.4
0.2	1015	$5x10^{20}$	0.650	10.4
0.3	780	$3x10^{20}$	0.940	11.1
0.4	630	$3x10^{20}$	1.260	8.3
0.5	530	$3x10^{20}$	1.570	6.6

Table I: Minimum emitter saturation current densities for metalized surfaces $J_{0e,met}$ and the corresponding surface peak doping concentrations, junction depths and sheet resistances obtained from numerical calculations in PC1D.

The value for the shallowest emitter and the best value differ by a factor of almost 3. This means, the shielding of the minorities in the emitter, the holes, from the metal-semiconductor interface has a strong impact on the resulting $J_{0e,met}$. The implications for a screen printed solar cell featuring a laser doped selective emitter are discussed in the next section.

Impact on solar cell performance

The results of the optimum value for $J_{0e,met}$ are investigated in a selective emitter solar cell structure. For this, the following structure is assumed: a 125x125 mm² monocrystalline solar cell, with a 2 Ωcm, 200 µm thick p-type base with an aluminum back surface field and 2 bus bars. Base and BSF are contributing J_{0b} = 500 fA/cm² to the total saturation current density J_{01}. A second diode recombination current of J_{02} = 20 nA/cm² is assumed as well as a generation of carriers leading to a short circuit current density of J_{SC} = 37 mA/cm². 100 µm wide metallization fingers are 2.0 mm spaced apart and a parallel resistance of R_P = 10 kΩcm² is assumed. The front side saturation current density J_{0e} is calculated by an area weighted mean of the illuminated emitter with a $J_{0e,ill}$ = 150 fA/cm² (at R_{sheet} = 100 Ω/sq) with the metalized fraction, in which the $J_{0e,met}$ (at 15 Ω/sq) is varied. For example, if 7% of the solar cell front side were covered with metallization, $J_{0e,met}$ contributes 7% to the total emitter saturation current density J_{0e}. For comparison, a future PERC device is also taken into consideration; it features an improved base (J_{0b} = 150 fA/cm²) and emitter ($J_{0e,ill}$ = 50 fA/cm²) at a finger width of 60 µm and a finger spacing of 1.6 mm. By using the 2-diode model [10],

$$J(V) = J_{01}\left(\exp\left(\frac{V - JR_S}{n_1 V_{th}} \right) - 1 \right) + J_{02}\left(\exp\left(\frac{V - JR_S}{n_2 V_{th}} \right) - 1 \right) + \frac{V - JR_S}{R_P} \qquad (4)$$

the open circuit voltage of that device is calculated. The results for J_{0e} and V_{OC} are shown in Table II.

$J_{0e,met}$ [fA/cm²]	Total J_{0e} of Al-BSF SP cell [fA/cm²]	V_{OC} of Al-BSF SP cell [mV]	Total J_{0e} of PERC cell [fA/cm²]	V_{OC} of PERC cell [mV]
3000	365	625.9	233	645.7
2000	291	628.0	171	649.8
1500	254	629.2	140	652.2
1000	217	630.4	110	654.8
500	180	631.7	79	657.7

Table II: Impact of the saturation current density of the metalized area on solar cell recombination, in terms of emitter saturation current density J_{0e} and open circuit voltage V_{OC} for the devices described in the text.

The values of $J_{0e,met}$ = 2000 and 3000 fA/cm² are obtained, if little or no shielding is provided for a shallow diffused emitter. These calculations show, that $J_{0e,met}$ can have a minor impact (~ 1% in V_{OC}) on the performance of the cell. However, when other recombination paths are eliminated in the cell, this impact can go up to 2% of the open circuit voltage. Thus, an improper choice of doping profile underneath the metal contact can result in a loss of efficiency of about 0.2%$_{abs}$ for η = 18.5% screen printed Al –BSF cell, or up to 0.4%$_{abs}$ for η = 19.5% PERC cell.

EXPERIMENTAL

Solar cells with selective emitters fabricated, featuring a 25/120 Ω/sq selective emitter. The processing sequence is shown in Figure 3. 200 µm thick, 125x125 mm² p-type Cz silicon with a base resistivity of 2 Ωcm was used. As a reference, solar cells with a homogenous emitter with a sheet resistance of R_{sheet} = 65 Ω/sq were also processed. For each emitter, an optimized grid was used. Laser doping was done with a frequency tripled Nd:YVO_4 DPSSL at a wavelength of λ = 355 nm and a pulse length of approximately τ_{Laser} = 25 ns. Two different pulse energies were chosen to achieve highly doped regions with sheet resistances of 26 and 23 Ω/sq, denoted in the following as low and high pulse energy E_P, respectively. The laser doped areas were chosen broad to insure a good alignment between the laser processed geometry and the screen printed metallization.

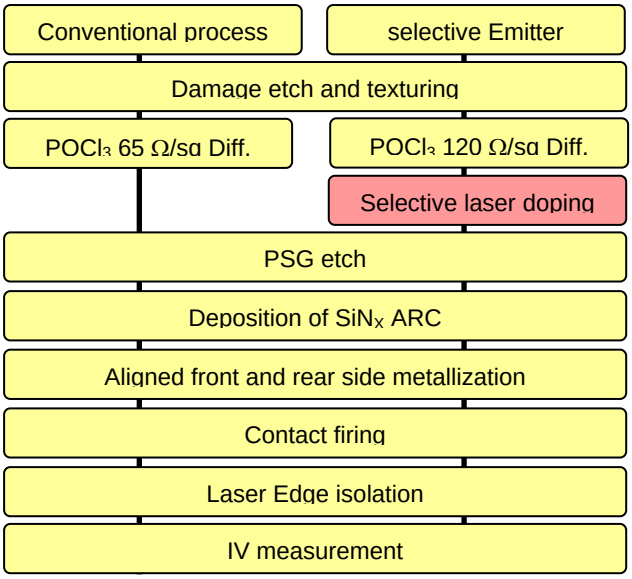

Figure 3: Processing sequence of the fabricated solar cells. As a reference, a batch of homogeneously doped solar cells with a sheet resistance of 65 Ω/sq was also processed.

RESULTS

Resulting profiles

Figure 4 depicts the doping profiles determined by a Secondary Ion Mass Spectroscopy measurement (SIMS). These profiles were acquired from laser doped samples on a shiny etched surface, which were laser processed with the same parameters as the solar cells. However, the pulse energy was adapted in order to achieve the same sheet resistance as on the alkaline textured surfaces.

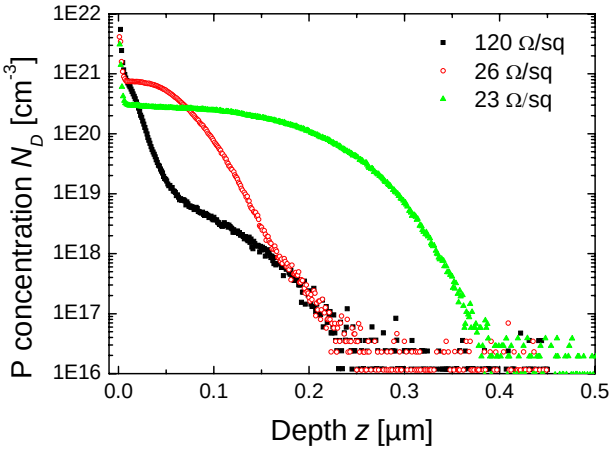

Figure 4: SIMS Profiles of the selective laser doped areas. For comparison, the shallow emitter with a sheet resistance of 120 Ω/sq emitter is also included.

For these profiles, the PC1D analysis as described above for $J_{0e,met}$ was performed and resulted in the values summarized in Table III. It can be seen, that the high doping to below 30 Ω/sq is beneficial for the suppression of $J_{0e,met}$. The authors noted that the program PC1D gave systematically too low values for the calculated sheet resistance via eq. (1). This is attributed to the parameterization of the mobility μ of the carriers. Masetti *et al.* presented investigations and a different parameterization for μ [11] which differs from the one used in PC1D at high doping. Using this mobility model, the agreement between the calculated sheet resistance from the doping profile and measured sheet resistance was better.

Emitter	120 Ω/sq	23 Ω/sq	26 Ω/sq
$J_{0e,met}$ [fA/cm²]	2900	1250	1900

Table III: PC1D analysis for the profiles in figure 4 to obtain $J_{0e,met}$

Open circuit voltage

Figure 5 shows the measured open circuit voltages V_{OC} for the processed solar cells. Selective emitter solar cells feature about 6 mV increase in V_{OC} compared to reference cell featuring a industrial homogeneous emitter. A notable difference in V_{OC} comparing the low and the high pulse energy can be observed. Although the sheet resistances of the two profiles seem comparable, i.e. 26 and 23 Ω/sq, the recombination properties on cell level exhibit differences. However, the expected difference of only 1-2 mV (see Table II and III) is exceeded.

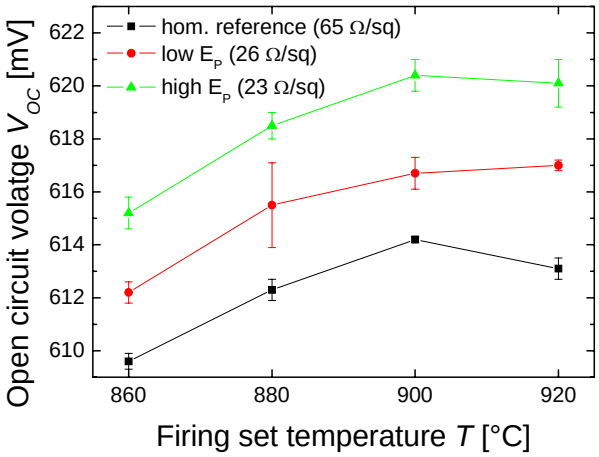

Figure 5: Open circuit voltages V_{OC} over firing set temperatures T for the processed solar cells. The data points represent the mean of 5 cells and the standard deviation is indicated by the error bars.

The dark IV data of the cells was fitted to the 2-diode-model (eq. (4)) with the ideality factors of the diodes fix at n_1=1 and n_2=2. The 2nd diode recombination current J_{02} was then extracted for the cells. For the reference cells and the cells with the high pulse energy, a value of J_{02} = 20 nA/cm² was determined.

The solar cells with the selective doping of 26 Ω/sq show an enhanced 2nd diode recombination current which is about 15-20 nA/cm² higher than for the reference cells and the cells processed with the high pulse energy.

An extended analysis was performed to see, whether the expected influence of $J_{0e,met}$ can be observed on cell level: The geometry of the processed cells was considered, the J_{0e} values of the highly doped, illuminated areas (26 Ω/sq: 1400 fA/cm² and 23 Ω/sq: 1200 fA/cm²) , as well as the value for the 120 Ω/sq (J_{0e} = 260 fA/cm²) emitter were measured in a separate experiment. These values were put into the calculation using the 2-diode-model. The value for J_{0b} was adapted to reproduce the measured open circuit voltage of the solar cells for the 23 Ω/sq selective doping at FFO temperature of 880°C. This is indicated by the two values in italics in Table IV. Then, the influence of J_{02} and $J_{0e,met}$ was subsequently applied to the cells and is shown in Table IV.

	FFO set T = 880°C V_{OC} [mV]		FFO set T = 900°C V_{OC} [mV]	
Sel. High doping	23 Ω/sq	26 Ω/sq	26 Ω/sq	26 Ω/sq
measured	*618.5*	615.5	620.4	616.7
J_{02} = 20 nA/cm²	*618.5*	618.5	620.3	620.3
J_{02} = 35 nA/cm²	--	617.1	--	618.9
With effect of $J_{0e,met}$	618.5	615.5	--	617.1

Table IV: Analysis of the losses induced by J_{02} and $J_{0e,met}$ employing the 2-diode-model. The values for J_{0b} were determined by adapting its value so the open circuit voltage of the IV measurements is reproduced for the solar cells at T=880°C with 23 Ω/sq selective doping.

The analysis reveals, that the reduction in the open circuit voltage V_{OC} for the shallower profile has two origins: partly it is due to an increased 2nd diode recombination current J_{02}, but also to a larger $J_{0e,met}$. The combined influence of J_{02} and $J_{0e,met}$ accounts correctly for the observed differences in the open circuit voltage.

This analysis was not performed for the fast firing set temperature of 900°C as signs of overfiring were visible and the value of J_{02} from the 2-diode-model fit was not considered to be reliable.

The authors also ascertained a strong impact of the doping profile on the short circuit current density of the solar cells. This is due to the inclusion of large alignment tolerances for the subsequent metallization process, as the highly doped area was chosen broad. However, so far the quantitative analysis of this effect did not yield the observed measurements. The authors attribute this to the fact, that the so far not determined recombination velocity S_{0p} of the nitride passivated, highly doped, illuminated area has a strong influence to the calculations in PC1D.

Investigations considering this aspect are ongoing, but the diminution of the alignment tolerances is highly beneficial for the solar cell, as less highly doped area is illuminated. This analysis is currently ongoing.

CONCLUSION

The influence of the doping profile underneath the metal contact for a laser doped selective emitter solar cell was investigated. An improper chosen doping profile can lead to insufficient suppression of the recombination at the metal-semiconductor interface. Solar cells reveal a dependence of the open circuit voltage on the doping profile. A shallower profile is detrimental, as both an increased J_{02} is observed for the cells and increased value of $J_{0e,met}$ leading to a lower V_{OC}.

ACKNOWLEDGEMENT

The authors thank Johannes Greulich for the fruitful discussions on the findings and Arthur Kremer for the support in the simulation.

REFERENCES

1. Ventura, L., A. Slaoui, and J.C. Muller. *Realization of selective emitters by rapid thermal and laser assisted techniques*. in *Proceedings of the 13th European Photovoltaic Solar Energy Conference*. 1995. Nice, France.
2. Röder, T., et al. *0.4% Absolute Efficiency Gain of Crystalline Silicon Solar Sells by Laser Doped Selective Emitters*. in *Proceedings of the 34th IEEE PVSC*. 2009. Philadelphia.
3. Jäger, U., et al. *Selective emitter by laser doping from phosphosilicate glass*. in *Proceedings of the 24th European Photovoltaic Solar Energy Conference*. 2009. Hamburg, Germany.
4. Fogarassy, E., et al., *A model for laser induced diffusion.* Journal of Applied Physics, 1983. **54**(9): p. 5059-63.
5. Clugston, D.A. and P.A. Basore. *PC1D version 5: 32-bit solar cell modeling on personal computers*. in *Proceedings of the 26th IEEE Photovoltaic Specialists Conference*. 1997. Anaheim, California, USA: IEEE; New York, NY, USA.
6. Solmi, S., et al., *Dopant and carrier concentration in Si in equilibrium with monoclinic SiP precipitates.* Physical Review B, 1996. **53**(12): p. 7836-41.
7. Wood, R.F., *Macroscopic theory of pulsed-laser annealing. III Nonequilibrium segregation effects.* Physical Review B, 1982. **25**(4): p. 2786-811.
8. Cuevas, A., et al., *Surface recombination velocity of highly doped n-type silicon.* Journal of Applied Physics, 1996. **80**(6): p. 3370-5.
9. King, R.R., R.A. Sinton, and R.M. Swanson, *Studies of diffused phosphorus emitters: saturation current, surface recombination velocity, and quantum efficiency.* IEEE Transactions on Electron Devices, 1990. **37**(2): p. 365-71.
10. Goetzberger, A., B. Voß, and J. Knobloch, *Sonnenenergie: Photovoltaik, Physik und Technologie der Solarzelle*. 2nd ed. 1997, Stuttgart: Teubner. 261.
11. Masetti, G., M. Severi, and S. Solmi, *Modeling of carrier mobility against carrier concentration in arsenic-, phosphorus-, and boron-doped silicon.* IEEE Transactions on Electron Devices, 1983. **30**(7): p. 764-9.